Fibers and Polymers 2021, Vol.22, No.10, 2689-2699
DOI 10.1007/s12221-021-0936-7

ISSN 1229-9197 (print version)
ISSN 1875-0052 (electronic version)

Palm Fibers Residues from Agro-industries as Reinforcement in Biopolymer Filaments for 3D-printed Scaffolds

Noelle Zanini[1], Emanuel Carneiro[2], Lívia Menezes[3], Hernane Barud[4]*, and Daniella Mulinari[1]*

[1]*Department of Mechanical and Energy, Technology College, Universidade do Estado do Rio de Janeiro, Resende, RJ 27537-000, Brazil*
[2]*Fluminense Federal University (UFF), Institute of Science and Technology, Rio das Ostras, RJ 28895-532, Brazil*
[3]*Macromolecules Institute (IMA), Federal University of Rio de Janeiro (UFRJ), Rio de Janeiro, RJ 21941-598, Brazil*
[4]*Department of Biotechnology, University of Araraquara (UNIARA), Araraquara, SP 14801-030, Brazil*
(Received August 10, 2020; Revised November 23, 2020; Accepted December 16, 2020)

Abstract: Poly(hydroxybutyrate-co-hydroxyvalerate) (PHBV) is a biodegradable, biocompatible, and non-toxic biopolymer. The biopolymer properties can be improved using cellulosic-based materials, often derived from agro-industrial residues, and promoting reuse/re-significance of a by-product for bone tissue engineering applications. Biocomposites of PHBV filled with bleached fibers of palm residues (BFPR) (0-10 % wt/wt) for 3D-printing were prepared. The scaffolds were obtained by additive manufacturing (fused deposition modeling (FDM)). The samples were characterized by stereomicroscopy, SEM, TGA, nanohardness, wettability, FTIR, and biocompatibility. Biocomposites filaments revealed homogeneous diameters, suitable for FDM. Composite filaments had thermal stability at 100-250 °C (processing did not degrade the material). The -OH groups of cellulose (enhanced by bleaching treatment) BFPR added to PHBV had advantages: optimal cell viability, wettability improvement, and slight nanohardness increase. PHBV/BFPR1 % scaffolds had an interconnected porous structure with a pore size of ~900 μm and 60 % filling.

Keywords: Biopolymer, Bleached fibers, Residue reuse, Additive manufacturing, Scaffold

Introduction

Tissue engineering applications in regenerative medicine are based on the production of three-dimensional (3D) scaffolds, which act as cellular support to guide tissue neoformation [1,2]. Additive manufacturing (AM), a 3D printing technology, has been considered one of the routes for obtaining scaffolds [3]. The most widely investigated AM technologies to make scaffolds are fused deposition modeling (FDM), stereolithography, selective laser sintering, direct-write, and binder jetting processes [4]. Besides being a cheap and affordable AM technique [5], FDM requires extruded polymeric filaments with specific dimensions can obtain interconnected porous structures and stable mechanical properties to mimic natural human bone [4,6].

The use of polymers to designed porous scaffolds is highlighted in the literature [7]. The fundamental properties of a scaffold material are biodegradability, bioactivity, and biocompatibility. Among the polymers available with those characteristics, the class of polyhydroxyalkanoate (PHA) is highlighted, in which poly(hydroxybutyrate-co-hydroxyvalerate) (PHBV) is a biopolymer of bacterial origin [8,9]. PHBV is a bio-based polyester of the PHA group and has a piezoelectric potential similar to bone tissue, aiding cell growth and regeneration [10]. Also, PHBV has surface chemistry that favors cell binding and proliferation [11]. As a copolymer, the addition of 3-hydroxyvalerate monomers to the poly (3-hydroxybutyrate) polymer chains can reduce the melting point to facilitate processing and promote improved mechanical properties if compared to PHB [12]. Despite the monomer's addition, PHBV may have low mechanical and thermal properties, processing difficulty, and high cost compared to petroleum-based plastics [13]. Thus, to minimize or eliminate such disadvantages, natural fiber has been used as reinforcement for its lightness, low price, biodegradability, and abundance [4,14].

Lignin, hemicellulose, and cellulose are the main components of natural fibers [15]. Surface treatments are often used in more than one step to extract the cellulose from the other components in natural fiber. Generally, an alkaline treatment is done first and then a bleaching treatment deeply removes lignocellulosic components, providing to the bleached fiber a light color and higher cellulose content [16]. Hickey and Pelling [17] mentioned that the study of cellulose-based materials should continue to grow as a trend due to the versatility/diversity of their biological traits for tissue engineering. *In vivo* applications of cellulosic-based biomaterials demonstrated positive effects such as the absence of an inflammatory response and compatibility with the living organism [18]. The use of cellulose in tissue engineering is made in several ways: regeneration of cartilage tissue, bone tissue, differentiation of endothelial cells, and dressings for superficial wounds [19]. Pei *et al*. [20] revealed that cellulose-based scaffolds made of acetate propionate reinforced with cellulose whiskers had similarities to human blood vessels' natural extracellular matrices. Such composite scaffolds presented improved mechanical properties

*Corresponding author: hernane.barud@gmail.com
*Corresponding author: dmulinari@hotmail.com

due to hydrogen bond strength and good cellulose-matrix dispersion. Therefore, as a cellulose-based material, bleached fibers can be used as reinforcement in scaffold applications [21]. In the literature, numerous works involve cellulose extraction from natural fibers [22-24].

Among the various fibers, palm fiber is an abundant by-product of agro-industries, with several applications [25,26]. The palm heart, also known as palmetto, can be extracted from various palm species. *Archontophoenix alexandrae* produces a noble type of the palm heart, with higher quality and superior flavor than other palm species [27]. Brazil is one of the largest producers/exporters/consumers of canned palm heart. Nevertheless, countries like Italy, Japan, France, and the USA also appreciate such delicacy [28]. The growing industrialization of palm heart extraction generates many agro-industrial residues since the commercial palm heart represents only 2 % of the palm tree [29]. These facts alert the urgent necessity for research on palm residues revaluing its agro-industrial byproduct, demonstrating that this work also has a concern in solid waste reuse.

This work presents a new perspective for Australian royal palm residues in FDM filaments for applications in scaffolds for regenerative medicine. Moreover, this work presents an interesting approach aligning the environmental re-signification of a natural residue, the surface treatment of natural fiber, the technology of AM for applications in tissue engineering using a PHBV composite. Herein, composite filaments of PHBV reinforced with bleached fibers of palm residues (BFPR) were developed and characterized, and scaffolds were designed and printed by fused deposition modeling (FDM). The filament samples were named PHBV/BFPR-X%, where the X stands for the BFPR content (from 0 to 10 % wt/wt).

Experimental

Materials

To obtain the composites filaments (1-10 % of BFPR), the fibers stem residues from the Australian royal palm tree were donated by Biosolvit (Volta Redonda, Brazil), and the PHBV from Biocycle 1000 was supplied by PHB Industrial S/A (Ribeirão Preto, Brazil), with the following characteristics: L110 lot, 91.93 % of PHB, 8.71 % of HV (hydroxyvalerate) and fusion temperature of 167.2 °C.

Obtaining Bleached Fibers of Palm Residues (BFPR)

To obtain the BFPR, the palm residues were oven-dried at 80 °C for 24 hours. After the physical processes of crushing and sieving (35 mesh or 500 μm), the untreated fiber of palm residues (UFPR) was obtained. The UFPR went through two surface treatments: alkaline treatment and bleaching. The alkaline treatment occurred when UFPRs were immersed in a solution of NaOH 4 % w/v to 70 °C for 1 hour. Then, they were filtered until reached neutral pH and oven-dried at 80 °C for 48 h. Then, the beaching process started: the fibers were mixed with NaOH solution 1 $mol \cdot l^{-1}$ to 70 °C, and were added H_2O_2 solution (30 %). The system was kept in agitation and under continuous heating, at 70 °C for 1 hour. They were then filtered to remove the excess of reagents, and all the bleaching steps were repeated. Furthermore, they were dried at 60 °C for 24 hours, obtaining the BFPR.

Preparation of PHBV/BFPR Filaments

Firstly, PHBV powder was mixed with BFPR. The filaments of PHBV reinforced with different percentages of BFPR (1 to 10 % wt/wt) were obtained using a mini-extruder (brand Weellzoom, model B Desktop, Guangdong Prov, China). The processing temperature of the filaments was in the range of 160-165 °C. The extrusion speed used was 380 mm/min. The mini-extruder (Weellzoom) has only one temperature control option, so different temperatures were not used throughout the extrusion chamber. According to the mini-extruder manufacturer, the diameter of the extrusion die is 1.75 mm, the extrusion rate is 254 mm/min, and the extrusion precision: +/- 0.05 mm (in 1.75 mm). The filament extrusion photo (S1) can be found in the Supplementary Material.

Characterization

Morphological and Microstructural Characterization

The morphology of the palm residues (UFPR and BFPR) and filaments (PHBV/BFPR-X%) was analyzed by Stereomicroscopy (SM) (brand ZEISS, model Axio Imager 2, New York, USA). The microstructure of the palm residues (UFPR and BFPR) and filaments (PHBV/BFPR-X%) were also analyzed by scanning electron microscopy (SEM) technique (Microscope brand HITACHI, Mannheim, Germany) with tungsten filament operating at 5 kV, employing a low-vacuum technique and secondary electron detector. Samples were dispersed on brass support and fixed with a double face 3M tape. For each micrograph of the cross-section fracture of the filaments, a randomly chosen BFPR was measured using the ImageJ (Maryland, USA) for diameter (D) and length (L) values.

Thermogravimetric Analysis (TGA)

TGA was performed to determine the thermal stability by the thermogravimetric curve (TG) of the palm residues (UFPR and BFPR) and filaments (PHBV/BFPR-X%), using a thermogravimetric analyzer (TA Instruments simultaneous TGA system, model SDT Q600, New Castle, USA). Experiments were carried out under continuous nitrogen flow, with a heating rate of 10 $^{o}C \cdot min^{-1}$ and specimen weight of 10 mg.

Fourier Transform Infrared Spectroscopy (ATR-FTIR)

The chemical structure of the palm residues (UFPR and BFPR) and filaments (PHBV/BFPR-X%) were evaluated by attenuated total reflectance ATR-FTIR (Perkin Elmer® Inc, model Spectrum 100, Massachusetts, USA). For all spectra,

16 scans were accumulated with a 4 cm^{-1} resolution.

Nanohardness

Nanohardness analysis was performed in PHBV/BFPR-X% filaments with a nanodurometer (DUH-W211S, Shimadzu Co., Tokyo, Japan) pyramidal diamond tip on 0.5 mm thick segments of the material. The material was subjected to indentation with a load of 0.01 mgf/msec, and subsequently, the indentation area generated for hardness calculation was measured.

Biocompatibility

To evaluate PHBV/BFPR-X% filaments' biocompatibility, a cytotoxicity assay was performed in L929 fibroblast lineage using standards of ISO 10993-5 and the methodology of Narayanamurthy *et al*. [30]. The cytotoxicity tests were carried out with samples in triplicate, and from them, an average was taken for each material. In this assay, L929 cell line fibroblasts were used and cultured in an essential medium supplemented with gentamicin and glutamine. These cell cultures were then kept at 37 °C and 5 % CO_2 to maintain cell viability. After contact with the materials, for time intervals of up to seven days, cell viability was measured based on the red dye absorption technique [30,31]. To each culture plate's aliquots, 10 μ*l* of a 0.01 % neutral red solution (Sigma Aldrich) was added. After dye addition, samples were incubated for 3 hours for dye penetration into viable cells. The absorption of the neutral red dye was then determined by measuring optical density (OD) on a spectrophotometer (BioTek, Winooski, Vermont, USA) with a wavelength of 492 nm. After analysis, the optical density data were compared with the standard, estimating the samples' cell viability difference as a percentage (considering the standard cells as 100 % viable). The data obtained were plotted using the OriginPro 2016 program. A contour diagram was made to ascertain the effect of two variables, fraction of BFPR (%) and a period of one week (seven days), generating a surface response of cell viability (%). The response surface method (RSM) combines different parameters and shows the static trend of the properties' behavior, with less than 10 % error [32].

Contact Angle

For contact angle (CA) analysis, films of PHBV/BFPR-X% were thermopressed with 8 ton, at first with the temperature of 165 °C for 2 min, and then at room temperature (25 °C) for 2 min (8-ton Hydro-Pneumatic Press, model Q/F 6066, Dehli, India). Subsequently, these films were analyzed on the Dataphysics Goniometer (Filderstadt, Germany), positioned below a syringe controlled by the SCA 20 software. The software was programmed to add 2 μ*l* of distilled and deionized water solvent to the samples' surface, and the CA point was measured after 5 seconds of contact between the solvent and the material.

Manufacture of Scaffolds by FDM Technique

The scaffolds were designed in TinkerCAD software in cylindrical format and printed by a Cliever model CL1 Black Edition 3D printer (Belo Horizonte, Brazil) with a 60 % filling and processing temperature of 170 °C. Then the scaffolds were 3D-printed according to the preset parameters and investigated by the SEM technique. A caliper ruler (brand Mitutoyo, model 500-196-20 Digimatic Digital) was used to measure the diameter and length of scaffolds. The ImageJ software (Maryland, USA) measured the scaffold pores. A video of the FDM printing of a scaffold (S2) can be found in the Supplementary Material.

Results and Discussion

Characterization

Morphological and Microstructural Characterization

The SM analysis evidenced modifications in the palm residues. The color variation of the UFPR (Figure 1a) after the surface treatment (BFPR, Figure 1b) is associated with the formation of chromophores groups due to the perhydroxyl ions (HOO-) generated by the dissociation of hydrogen peroxide in alkaline media, which were responsible for the decolorization of the palm residues in the bleaching treatment. These ion attacks of the bleaching process removed the chromophore compounds of the remaining hemicellulose and lignin in the delignification process (shown in the graphical representation of UFPR and BFPR in Figure 1). Thus, the fiber became whiter and might produce better physical and thermal characteristics [33,34].

The addition of BFPR to the biopolymer matrix increased the opacity in the filaments (Figure 1c to Figure 1h) as expected and comparable to the literature [35], and may have caused friction in the extrusion by higher surface agglomeration (altering the material viscosity), as seen by the whitish areas on the PHBV/BFPR-7.5 % and PHBV/BFPR-10 % surface (Figure 1g and Figure 1h, respectively). The round shape of the filaments presented a nominal diameter between 1.60 to 1.62 mm, slightly small than the diameter of the commercial FDM filaments (1.75 mm) [36], but still suitable for the FDM technique.

The surface treatments in palm residues also altered the morphology, as shown in the micrographs by the SEM technique (Figure 1i to Figure 1j). The UFPR morphology demonstrated the accumulation of fibers in layers with a homogeneous surface (Figure 1i). In the BFPR, defibrillation was observed due to the surface bleaching treatment, which promoted fiber individualization (Figure 1j). This change occurs due to removing surface impurities, lignin, and hemicellulose (as seen by the graphical representation of BFPR in Figure 1). Moreover, the BFPR presented irregular geometry and rough surface [25], facilitating fiber impregnation in the PHBV matrix.

The insertion of BFPR to the PBHV modified the filament microstructure. Montanheiro *et al*. [9] found similar micrographs of PHBV composite filaments. In this work, The PHBV/

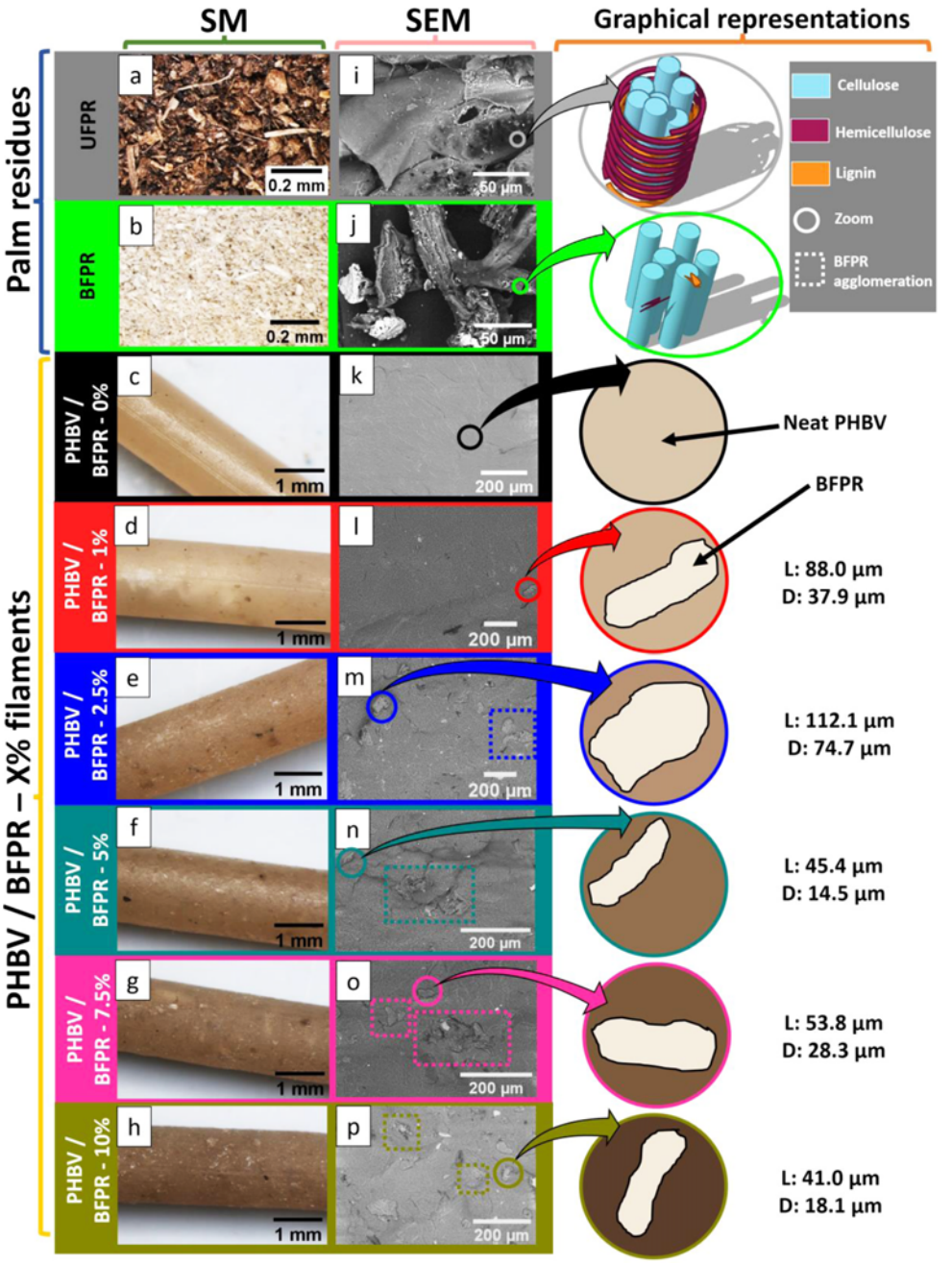

Figure 1. SM, SEM, and graphical representations of the samples.

BFPR-0 % filament presented a solid cross-section without visible voids (Figure 1k). Nevertheless, the addition of the BFPR led to visible pores in the filament (darker areas). The BFPR was found in the micrographs of all PHBV/BFPR filaments (Figure 1l to Figure 1p), dispersed randomly (agglomerated or isolated), non-impregnated, and impregnated in the biopolymer. Additionally, stress concentration regions and voids around BFPR were seen, which could affect the properties by microcrack formation [37]. The PHBV/BFPR-10 % filament fracture (Figure 1p) presented a less homogeneous surface with a large agglomeration of BFPR. Despite the fiber agglomerations, the L and D of the BFPR (randomly chosen in the cross-section of the filaments and represented graphically) possibly mean that the surface treatments decreased the fibers' dimensions. The palm residues initially passed through the 500 µm sieve, and in the micrographs, the BFPRs have L between 88-48 µm and D between 14.5-37.9 µm.

TGA

TG curves of palm residues (UFPR and BFPR) and filaments (PHBV/BFPR-X%) were achieved by thermogravimetric analysis (Figure 2). The curves related to palm residues demonstrated two weight loss events; the first one from room temperature up to 130 ºC is attributed to water evaporation, while the second one relates to degradation of hemicellulose, lignin, and cellulose [38]. On the other hand, the addition of BFPR to the biopolymer leads to increased degradation. The T_{onset} of the PHBV/BFPR+X% filaments reduced with the addition of BFPR (Figure 2b).

From the data in Table 1, the composite filaments exhibited stability between 100 and 250 °C, not exceeding 1.5 % of mass loss. Thermal stability plays an important role in biopolymer melt processing due to their characteristic narrow processing window [39]. Filaments extrusion and FDM print occurred in the range of 160 to 170 °C, so thermal properties have not been compromised with the addition of BFPR. Temperatures that exceed this range were also studied for investigative purposes, to study the thermal behavior at 100 ° intervals and the remaining residue at the end of the analysis. From 270 °C, a large loss of the composites filaments mass was noted, with emphasis on PHBV/BFPR-10 %, as seen in the first zoom (Figure 2c). The residue produced after TGA analysis for PHBV/BFPR-0 % was 0.71 %, while BFPR was 36.46 %. The adding BFPR to the biopolymer matrix caused an increase in the residue percentage, also noted by the reduced mass loss at the 400-500 °C range of filaments with higher BFPR content. Hassan *et al.* [40] observed similar behavior in kenaf fiber reinforced PHB composites. Likewise, after 250 °C, a decrease in mass percentage occurred in PHBV/BRPR-0 % filaments, accentuated with BFPR high percentages, as evidenced in other studies [41,42]. A slight disturbance before 400 °C as a second event was also observed in composites filaments with a higher fiber amount (PHBV/BFPR-7.5 % and PHBV/-BF-10 %), possibly by BFPR acting on the composite filament thermal behavior.

Fourier Transform Infrared Spectroscopy (ATR-FTIR)

Through the FTIR technique, it is possible to identify, through functional groups, modifications resulted from the superficial treatments of palm residues (Figure 3a) and the influence of BFPR in the PHBV matrix (Figure 3b). The band 1603 cm^{-1} and 1233 cm^{-1} (attributed to C=C bond in

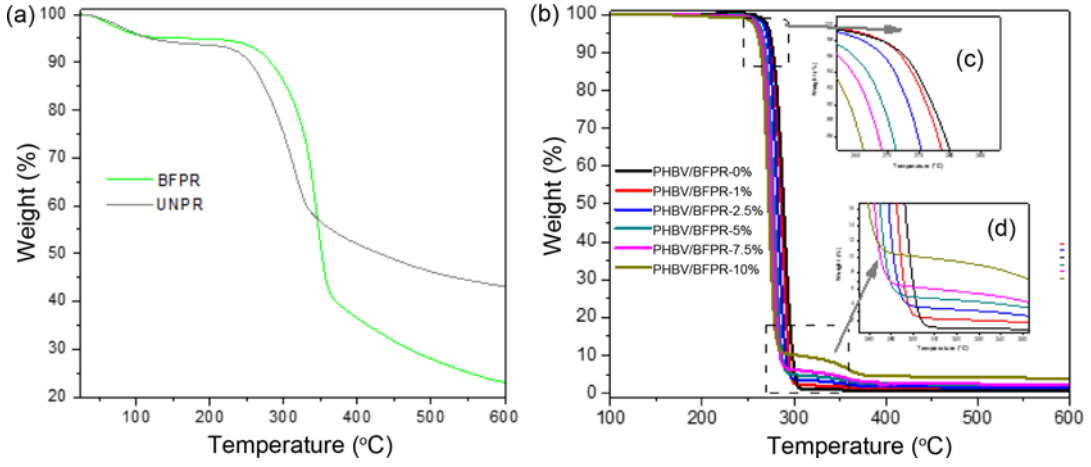

Figure 2. Thermogravimetric curves of the (a) palm residues (UFPR and BFPR), (b) PHBV/BFPR-X% filaments, (c) the first zoom, and (d) the second zoom.

Table 1. Mass loss, residue, and degradation temperature of palm residues (UFPR and BFPR) and PHBV/BFPR-X% filaments

Sample	Mass loss (%)						Residue (%)	Degradation temperature (°C)
	100 °C	200 °C	250 °C	300 °C	400 °C	500 °C		
UFPR	4.05	6.40	9.32	15.89	25.17	48.04	51.96	316.13
BFPR	4.23	5.14	6.30	8.81	14.01	63.54	36.46	345.81
PHBV/BFPR-0 %	0.0	0.0	0.0	6.78	94.69	99.29	0.71	287.45
PHBV/BFPR-1 %	0.0	0.0	0.24	8.85	97.24	98.77	1.23	287.37
PHBV/BFPR-2.5 %	0.0	0.0	0.07	14.07	96.22	98.13	1.87	282.89
PHBV/BFPR-5 %	0.0	0.0	0.33	32.77	95.05	97.43	2.57	277.89
PHBV/BFPR-7.5 %	0.0	0.11	0.57	46.27	93.76	97.57	2.43	276.19 / 354.64
PHBV/BFPR-10 %	0.0	0.38	1.27	68.68	89.91	95.39	4.61	272.14 / 360.02

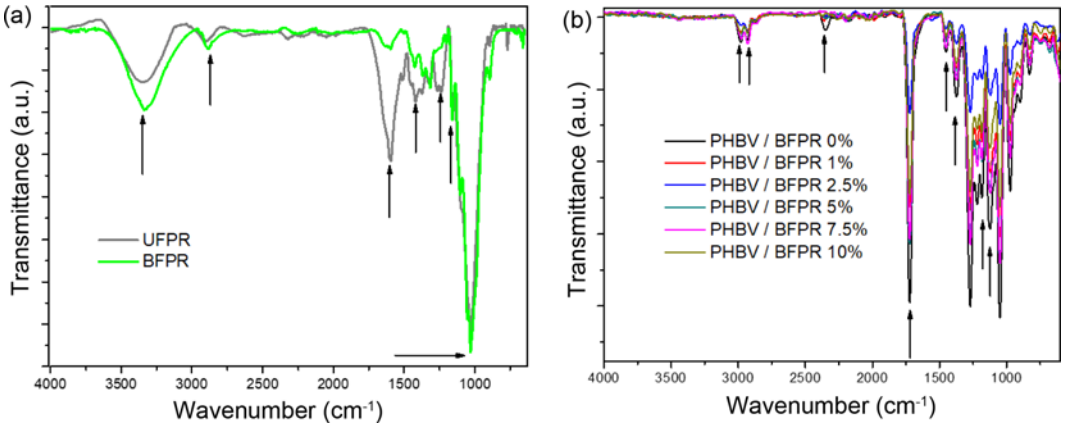

Figure 3. FTIR graph of the (a) palm residues (UFPR and BFPR) and (b) PHBV/BFPR-X% filaments.

aromatic rings in lignin and the C-C-O stretching lignin, respectively) reduced after the surface treatment for BFPR. [25].

Other characteristic bands of lignocellulosic materials were found: 2885 cm^{-1} (C-H group), 1427 cm^{-1} (CH_3 group), 1163 cm^{-1} (C-H stretching of cellulose), and 1033 cm^{-1} (C-C stretching) [43,44]. The band between 3500 and 3200 cm^{-1} increased after bleaching and corresponds to the cellulose -OH group. The -OH group band is related to the bleaching process, which removed non-cellulosic components, increasing the fibers' hydrogen forces.

The PHBV/BFPR-X% bands were similar, and possibly, the BFPR did not perform strong chemical interactions with the biopolymer matrix (Figure 3b). Some characteristic bands for PHBV decreased after BFPR insertion in the matrix and can be proof of weak interactions with BFPR: an accentuated band of 1722 cm^{-1} was observed for the C=O ester carbonyl stretch (characteristic of polyesters); band at 1128 cm^{-1} for axial and angular C-C stretches; band at 1190 cm^{-1} symmetrical or non-symmetrical C-O-C stretches; bands at 1379 cm^{-1} and 1458 cm^{-1} of symmetric C-H deformation of the methyl group; bands at 2931 and 2978 cm^{-1} angular deformation of the C-H bond of the methyl group [45].

Weak fiber/matrix interaction in the composite filaments was also observed by nanohardness.

Nanohardness

Figure 4 shows the Nanohardness values for the PHBV/BRPR-X% filaments. A hardness range between 260 and 270 MPa was found for the filaments. The addition of BFPR to PHBV exhibited a slight increase compared to the PHBV/BFPR-0 %, except the PHBV/BFPR-10 %. The composite filaments presented higher standard deviation values than PHBV/BFPR-0 % since the BFPR enhanced the variation between the nanohardness values for each sample but did not tend to grow with higher BFPR loadings [46].

The hardness in the PHBV/BFPR-X% had little influence

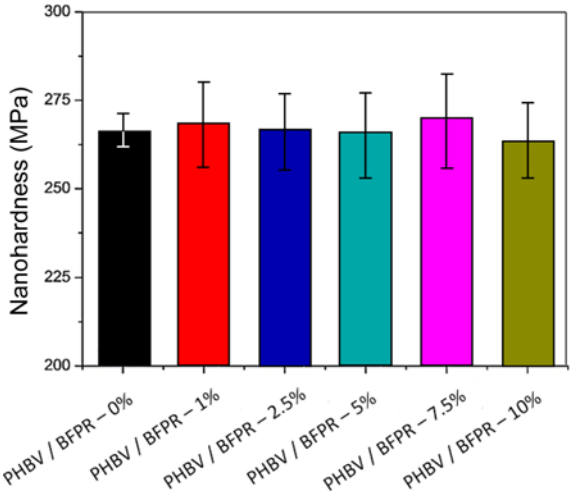

Figure 4. Nanohardness graph of the PHBV/BFPR-X% filaments.

by BFPR addition. Then, factors may have acted together for such results: i) the palm residue's amorphous nature, ii) the biopolymer crystallinity, and iii) the cellulose non-modification. Firstly, the palm residue's organic origin contributed to a lower hardness of BFPR (compared to inorganic particles, for example), resulting from the less organized structure of these fibers and the existence of amorphous nature. Another factor was the relatively high crystallinity of PHBV [47], which already contributed to these biopolymers' higher brittleness [48]. Lastly, the absence of BFPR modification limited biopolymer/fiber interaction and adhesion, as indicated by the FTIR technique, which may difficult improvements in the materials' mechanical properties.

Although weak adhesion between the fiber/matrix may seem disadvantageous from the mechanic's point of view, good bioactivity (Figure 5) of the materials was noted due to the OH groups of BFPR (as seen by FTIR) involved with the biopolymer matrix and displayed on the surface of the scaffolds, facilitating the process of calcium deposition on

the surface of these materials when in contact with body fluid [49,50].

Biocompatibility

An important analysis, often used to determine the material behavior in body fluids, was cytotoxicity, determining the biocompatibility (Figure 5). After seven days of contact (the PHBV/BFPR-X% samples with L929 cells), cell viability remained above 95 % for all systems evaluated (Figure 5a). These findings classify all samples as biocompatible materials based on ISO 10993-5, which regulate the behavior required of materials for application in the human organism. As the biopolymer matrix, such an outcome was expected, for in other studies, high biocompatibility of PHA's was evidenced (due to their chain structure without cyclic structures or clusters, which did not exist in proteins of the human organism) [51,52]. Moreover, those studies emphasized that products derived from the PHA's degradation do not have toxic characteristics and can be spontaneously eliminated from the body. Therefore, the composites filaments were suitable for their application in tissue engineering, and BFPR did not present acidic or basic residues of their obtaining process, so the purity of the samples did not damage the cell units in contact with the material.

The effect of both time (days) and the fraction of BFPR on the composite filament samples was seen through the contour diagram's surface response (Figure 5b). The BFPR fraction did not obtain linearity in its cell viability data over the days. The largest fiber fractions (in the range of 7 to 10 %) obtained optimal cell viability (above 95 %) for all analysis days. The fiber fraction in the range between 2 and 4 % obtained the lowest cell viability values on the sixth day but reversed this situation on the seventh day. Thus, the largest fractions of BFPR (from 7 to 5 %) have more stable cell viability in the analysis period, but all samples reached 95 % of cell viability (or more) after seven days. Figure 1c represents a graphical representation of the cytotoxicity

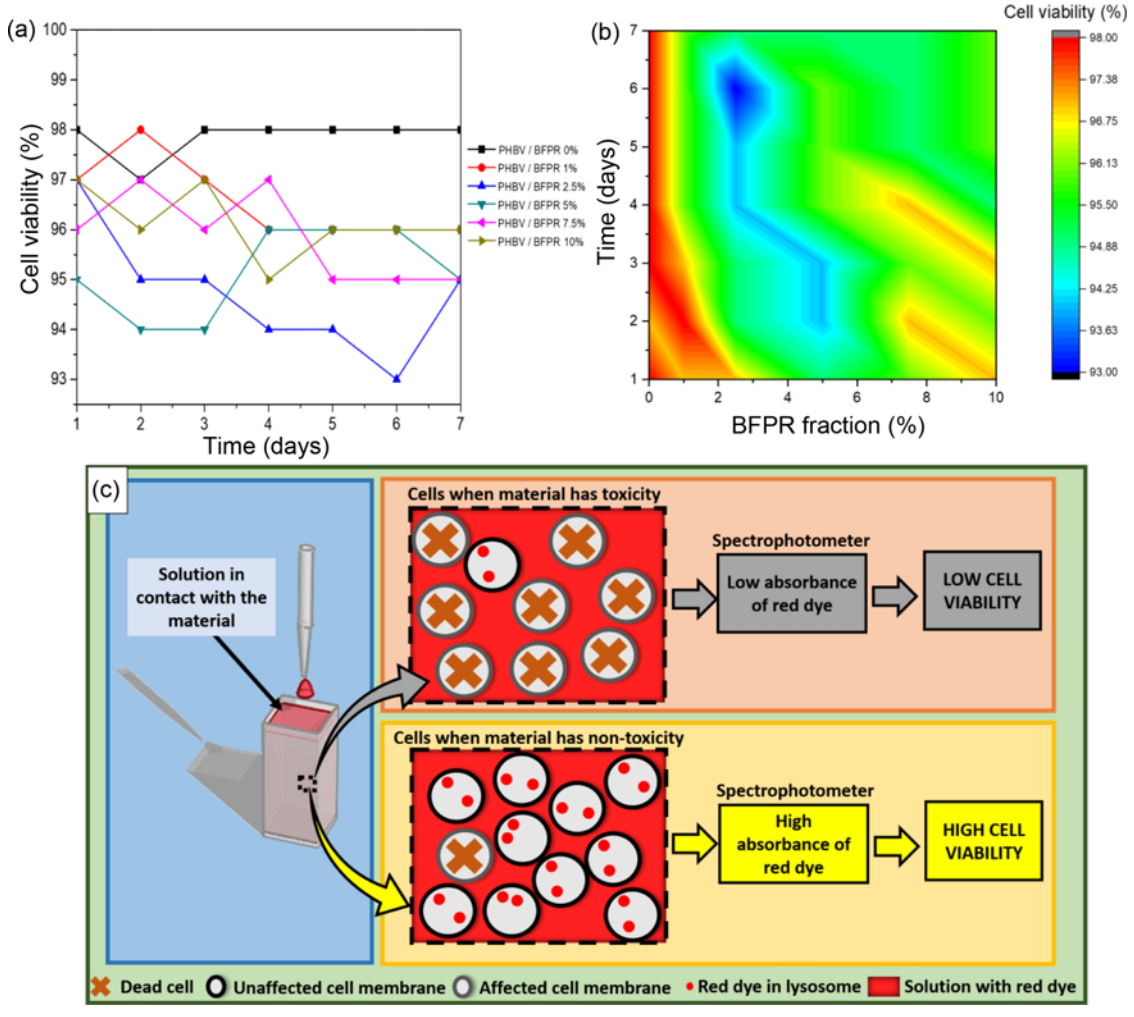

Figure 5. (a) Cytotoxicity graph of the PHBV/BFPR-0 % filaments, (b) contour diagram demonstrating the effect of BFPR fraction (1-10 %) for each day of analysis in the cell viability, and (c) red dye adsorption for determining cell viability. A graphical representation of two situations: when the material is toxic and when the material is non-toxic.

assay and the effect of non-toxic and toxic materials for cells that encountered the analysis material. The lysosomes of living cells absorb the red dye, which has a specific wavelength identified by the spectrophotometer.

Contact Angle

The contact angle (CA) is also a fundamental analysis and verify the wettability of a material. If the angle between the water drop of the analysis and the material's surface is greater than 90 °, it is a hydrophobic material. However, if the angle is smaller than 90 °, it is a hydrophilic material (with good wettability) [53]. Surface wettability analysis of the material was necessary to establish its behavior when in contact with plasma and other extracellular matrices rich in human tissues. Regarding the CA, all samples can be classified as having hydrophilic surfaces, with contact angles below 90º (Figure 6a). Furthermore, the addition of BFPR to the biopolymer improved surface wettability, and for fractions above 5 % BFPR, the difference was statistically significant. While the PHBV/BFPE-0 % sample obtained θ=76.7±2.5 the sample with the highest percentage of BFPR, PHBV/BFPR-10 % obtained θ=56.2±3.0 ° (Figure 6b). Those outcomes favor the interaction of the material with water. The presence of the -OH groups of the natural fibers, in this case from palm residues, exposed on the fiber surface, promoting hydrophilic behavior [54], as seen by FTIR analysis.

The wetting behavior can influence the osteoconductivity of bone-substituting biomaterial [55]. The wettability increase is fundamental for the material purpose (scaffolds). The literature confirms that wettability favors greater interaction of the frameworks with the biological environment, facilitating the salt and protein deposition processes on the scaffold surface. Moreover, the increase of wettability could help the cell adhesion process, evidencing that the addition of BFPR may compensate for the hydrophobic characteristic of PHA's [56].

Manufacture of Scaffolds by FDM Technique

As wettability and biocompatibility, the scaffold pores are also essential to cell proliferation and adhesion, acting as structural support for new tissue growth [57,58]. The scaffolds obtained by the FDM technique can be seen in Figure 7. Due to the addition of BFPR to the biopolymer matrix, it was only possible to print the PHBV/BFPR-0 % and the PHBV/BFPR-1 % filament. Higher reinforcement percentages caused the printer nozzle to clog (diameter 0.4 mm) due to agglomerations of BFPR, as seen by SM and SEM (higher surface agglomeration altering the material viscosity, especially in PHBV/BFPR-10 % surface (Figure 1h and Figure 1p).

Nonetheless, the scaffolds had close to expected diameters (4 mm thickness and 15 mm diameter) and resembled other studies in the literature (Figure 7a and 7b) [59,60]. The surface morphology and microstructure of the prepared scaffolds was also explored by SEM (Figure 7c and 7d). The SEM investigation showed an interconnected pore network, increasing fluid/nutrients facilitating scaffold vascularization [61]. Pilia *et al*. [62] mentioned that the ideal scaffold characteristics for bone tissue engineering applications are a pore size range of 300-900 μm and porosity in the range of 60-90 %. One of the parameters used in FDM printing was 60 % filling, and the ImageJ software also found pore sizes of ~900 μm, as previously computer-aided designed. These findings made the printing scaffolds promising for bone tissue engineering.

Future Works and Challenges

As future works, it would be necessary to investigate the following items: UFPR purity analysis, mechanical properties in the scaffolds printed by FDM through compression tests; the dispersion of the BFPR in the biopolymer matrix of the printed scaffolds through a better method of the mixture (thermokinectic mixer, as an example) and how they affect the scaffold porosity, and the applications of scaffolds *in vitro* and *in vivo* studies.

Despite the excellent cell viability for higher BFPR fractions, the challenge in future works would be to study

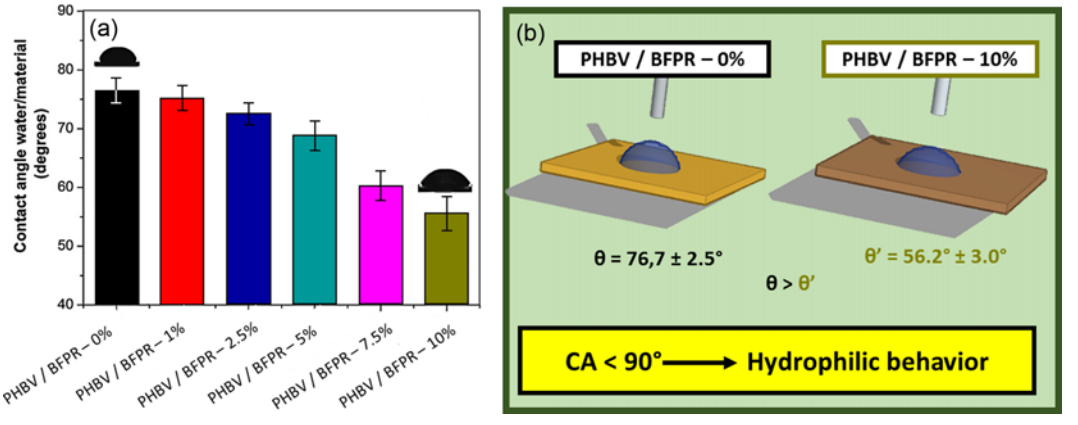

Figure 6. (a) CA graph of the PHBV/BFPR-X% filaments and (b) graphical representation of CA analysis and the difference between PHBV/BFPR-0 % and PHBV/BFPR-10 % values.

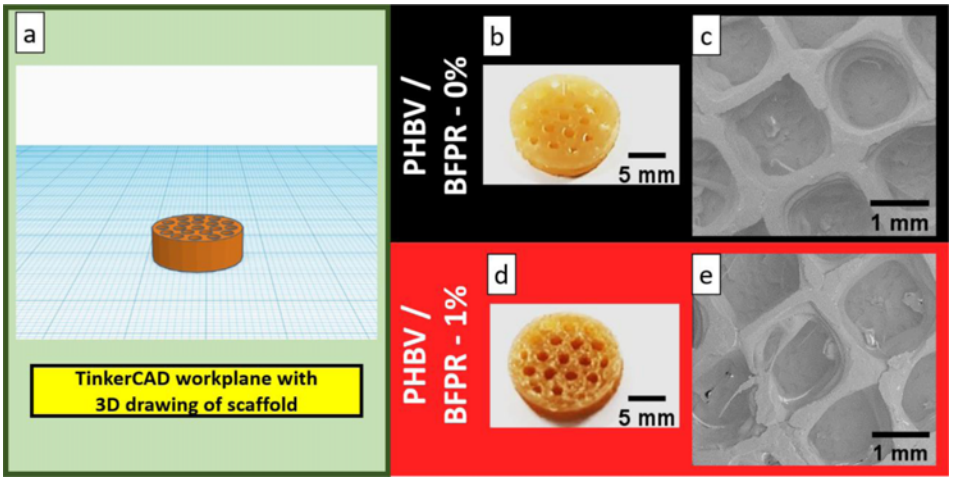

Figure 7. (a) TinkerCAD software for scaffold design and the designed scaffold in the software workplane; PHBV/BFPR-0 % scaffold (b) photo and (c) SEM; PHBV/BFPR-1 % scaffold (d) photo and (e) SEM.

non-agglomeration of fibers in the nozzles of the filament processing techniques (mini-extruder, and more importantly, in the FDM printer). A nozzle with a larger diameter or the use of BFPR in nanometric dimensions might be the alternatives. The literature has already revealed that incorporating of nanoparticles in polymeric matrices could improve mechanical and thermal properties for tissue engineering applications [63]. Although the preliminary characterization made in this work is not necessary for the validation of the obtained biocomposites, PHBV with UFPR can be an interesting material for bone tissue engineering.

Conclusion

Through the SM analysis, the surface treatment on the palm residue's untreated fiber (UFPR) provided discoloration, and the bleached fibers of the palm residue (BFPR) became lighter. In the PHBV/BFPR-X% filaments, the addition of BFPR made them darker, opaque, linear, and with suitable diameters for FDM. From the SEM images, the bleaching caused an individualization of fibrils in BFPR. However, a tendency of fiber agglomeration was observed with the increase of BFPR in the PHBV matrix, causing tension concentration (filament rupture) and clogging of the FDM printer nozzle (which was later proven). The TG of the composite filaments indicated thermal stability at 100-250 °C (extrusion and FDM printing did not degrade the material). The FTIR analysis revealed that the bleaching increased the band of the cellulose -OH group in the BFPR, allowing interactions with the biopolymer. However, for PHBV/BFPR-X% filaments, no strong changes were seen with the addition of BFPR, only a slight decrease in the characteristic bands of PHBV (weak fiber-matrix interaction). Nanohardness indicated a slight increase with the gradual insertion of BFPR in PHBV (except for PHBV/BFPR-10 %), corroborating with FTIR. By the cytotoxicity assay, cell viability was above 95 % after seven days. Thus, all samples can be considered biocompatible. The contour diagram showed that the largest BFPR fractions had more stable cell viability at all days of analysis. The composite filaments proved to be hydrophilic, an essential property for its application in living organisms' fluids. BFPR improved the material's wettability, with the PHBV/BFPR-10 % sample being the most hydrophilic (due to the more present -OH groups of cellulose). Only the PHBV/BFPR-0 % and PHBV/BFPR-1 % scaffolds were printed, while the other BFPR percentages caused the FDM printer nozzle to clog. Despite the BFPR agglomerations, the FDM printed scaffolds presented ideal bone tissue materials: interconnected pores (900 μm) and 60 % filling. Thus, surface treatments of palm waste as a filler in biopolymers are promising for bone tissue engineering. The reframing of an agro-industrial by-product, a cellulose-based bleached fiber, provides a different approach for Australian royal palm residues in the field of regenerative medicine. Nonetheless, improvements and studies on PHBV/BFPR scaffolds' properties would be necessary, also *in vivo* and *in vitro* applications.

Acknowledgment

The authors are grateful for the research support by FAPERJ (Process 260.026/2018) and the company Biosolvit for the donation of royal palm fibers.

Electronic Supplementary Material (ESM) The online version of this article (doi: 10.1007/s12221-021-0936-7) contains supplementary material, which is available to authorized users.

References

1. C. Meng, J. Zhao, Y. Yin, J. Luo, L. Zhao, W. Jiang, and J. Feng, *Fiber. Polym.,* **21**, 709 (2020).
2. E. L. Cyphert, M. Bil, H. A. von Recum, and W. Święszkowski, *J. Biomed. Mater. Res. - Part A,* **108**, 1144 (2020).
3. S. Radhakrishnan, S. Nagarajan, M. Bechelany, and S. N. Kalkura in "Processes and Phenomena on the Boundary Between Biogenic and Abiogenic Nature" (O. Frank-Kamenetskaya, D. Vlasov, E. Panova, and S. Lessovaia Eds.), pp.3-19, Springer, Cham, 2020.
4. V. K. Balla, K. H. Kate, J. Satyavolu, P. Singh, and J. G. D. Tadimeti, *Compos. Part B Eng.,* **174**, 106956 (2019).
5. G. Choi and S. Kim, *Fiber. Polym.,* **17**, 977 (2016).
6. S. Xia, Z. Song, P. Jeyakumar, S. M. Shaheen, J. Rinklebe, Y. S. Ok, N. Bolan, and H. Wang, *Crit. Rev. Environ. Sci. Technol.,* **49**, 1027 (2019).
7. A. I. Aghmiuni, M. S. Baei, S. H. Keshel, and A. A. Khiyavi, *Fiber. Polym.,* **21**, 33 (2020).
8. G. R. de Almeida Neto, M. V. Barcelos, M. E. A. Ribeiro, M. M. Folly, and R. J. S. Rodríguez, *Mater. Sci. Eng. C,* **104**, 110004 (2019).
9. T. L. de A. Montanheiro, F. H. Cristóvan, J. P. B. Machado, D. B. Tada, N. Durán, and A. P. Lemes, *J. Mater. Res.,* **30**, 55 (2014).
10. M. L. Tebaldi, A. L. C. Maia, F. Poletto, F. V. de Andrade, and D. C. F. Soares, *J. Drug Deliv. Sci. Technol.,* **51**, 115 (2019).
11. S. H. Diermann, M. Lu, G. Edwards, M. Dargusch, and H. Huang, *J. Biomed. Mater. Res. - Part A,* **107**, 154 (2019).
12. A. Anžlovar, A. Kržan, and E. Žagar, *Arab. J. Chem.,* **11**, 343 (2018).
13. L. J. Vandi, C. M. Chan, A. Werker, D. Richardson, B. Laycock, and S. Pratt, *Polym. Degrad. Stab*., doi: 10.1016/j.polymdegradstab.2018.10.015 (2019).
14. E. Diabor, P. Funkenbusch, and E. E. Kaufmann, *Fiber. Polym.,* **20**, 217 (2019).
15. L. N. Ludueña, A. Vecchio, P. M. Stefani, and V. A. Alvarez, *Fiber. Polym.,* **14**, 1118 (2013).
16. C. C. Hernandez, F. F. Ferreira, and D. S. Rosa, *Carbohydr. Polym.,* **193**, 39 (2018).
17. R. J. Hickey and A. E. Pelling, *Front. Bioeng. Biotechnol*., doi: 10.3389/fbioe.2019.00045 (2019).
18. X. Zhang, C. Wang, M. Liao, L. Dai, Y. Tang, H. Zhang, P. Coates, F. Sefat, L. Zheng, and J. Song, *Carbohydr. Polym.,* **213**, 27 (2019).
19. N. O'Donnell, I. A. Okkelman, P. Timashev, T. I. Gromovykh, D. B. Papkovsky, and R. I. Dmitriev, *Acta Biomater.,* **80**, 85 (2018).
20. B. Pei, W. Wang, Y. Fan, X. Wang, F. Watari, and X. Li, *Regen. Biomater.,* **4**, 257 (2017).
21. N. T. Lam, R. Chollakup, W. Smitthipong, T. Nimchua, and P. Sukyai, *Ind. Crops Prod.,* **100**, 183 (2017).
22. S. Ventura-Cruz, N. Flores-Alamo, and A. Tecante, *Int. J. Biol. Macromol.,* **155**, 324 (2020).
23. I. Gulati, J. Park, S. Maken, and M. G. Lee, *Fiber. Polym.,* **15**, 680 (2014).
24. D. C. Marin, A. Vecchio, L. N. Ludueña. D. Fasce, V. A. Alvarez, and P. M. Stefani, *Fiber. Polym.,* **16**, 285 (2015).
25. W. A. Paixão, L. S. Martins, N. C. Zanini, and D. R. Mulinari, *J. Inorg. Organomet. Polym. Mater.,* **30**, 2591 (2019).
26. I. R. Dantas, N. C. Zanini, J. P. Cipriano, M. R. Capri, and D. R. Mulinari in "Advances in Natural Fibre Composites" (R. Fangueiro and S. Rana Eds.), pp.51-59, Springer, Cham, 2018.
27. J. Guedes, W. M. Florentino, and D. R. Mulinari, "Design and Applications of Nanostructured Polymer Blends and Nanocomposite Systems", pp.55-73, Elsevier Inc., Amsterdam, 2016.
28. L. D. E. Araujo, N. G. Pimenta, M. F. Bergmann, A. V. Pinto, R. Battisti, and E. C. Leopoldino, *Rev. Técnico Científica do IFSC*, **2.9**, 11 (2020).
29. R. D. S. Zenni, C. V. Helm, and L. B. B. Tavares, *Rev. Gestão Sustentabilidade Ambient.,* **7**, 276 (2018).
30. V. Narayanamurthy, F. Samsuri, A. Y. F. Khan, H. A. Hamzah, M. B. Baharom, T. Kumary, A. Kumar, and D. K. Raj, *Bioinspiration Biomimetics*, **15**, 016002 (2019).
31. P. Slepička, J. Siegel, O. Lyutakov, N. S. Kasálková, Z. Kolská, L. Bačáková, and V. Švorčík, *Biotechnol. Adv.,* **36**, 839 (2018).
32. M. Gandara, D. R. Mulinari, F. M. Monticeli, M. R. Capri, D. R. Mulinari, and F. M. Monticeli, *J. Nat. Fibers*, doi.org/10.1080/15440478.2019.1710653 (2020).
33. G. Basu, L. Mishra, and A. K. Samanta, *J. Nat. Fibers*, **16**, 442 (2019).
34. A. S. Fonseca, S. Panthapulakkal, S. K. Konar, M. Sain, L. Bufalino, J. Raabe, I. P. A. Miranda, M. A. Martins, and G. H. D. Tonoli, *Ind. Crops Prod.,* **131**, 203 (2019).
35. L. Hilliou, P. F. Teixeira, D. Machado, J. A. Covas, C. S. S. Oliveira, A. F. Duque, and M. A. M. Reis, *Polym. Degrad. Stab.,* **128**, 269 (2016).
36. S. I. Atsani and H. Mastrisiswadi, *IOP Conf. Ser. Mater. Sci. Eng.,* **722**, 012022 (2020).
37. Z. Hu, Q. Shao, Y. Huang, L. Yu, D. Zhang, X. Xu, J. Lin, H. Liu, and Z. Guo, *Nanotechnology*, **29**, 185602 (2018).
38. M. Kathirselvam, A. Kumaravel, V. P. Arthanarieswaran, and S. S. Saravanakumar, *Carbohydr. Polym.,* **217**, 178 (2019).
39. O. A. Adeyeye, E. R. Sadiku, A. B. Reddy, A. S. Ndamase, G. Makgatho, P. S. Sellamuthu, A. B. Perumal, R. B. Nambiar, V. O. Fasiku, and I. D. Ibrahim in "Green Biopolymers and Their Nanocomposites" (D. Gnanasekaran Ed.), pp.221-231, Springer, Singapore, 2019.
40. A. Hassan, M. R. M. Isa, and Z. A. M. Ishak, *BioResources*, **14**, 3101 (2019).
41. T. Zheng, Z. Zhang, S. Shukla, S. Agnihotri, C. M.

Clemons, and S. Pilla, *Carbohydr. Polym.,* **205**, 27 (2019).
42. K. Yorseng, N. Rajini, S. Siengchin, N. Ayrilmis, and V. Rajulu, *Process Saf. Environ. Prot.,* **124**, 187 (2019).
43. M. J. Halimatul, S. M. Sapuan, M. Jawaid, M. R. Ishak, and R. A. Ilyas, *Polimery/Polymers*, **64**, 596 (2019).
44. S. M. Izwan, S. M. Sapuan, M. Y. M. Zuhri, and A. R. Mohamed, *J. Mater. Res. Technol.,* **9**, 5805 (2020).
45. N. Thakor, U. Trivedi, and K. C. Patel, *Bioresour. Technol.,* **96**, 1843 (2005).
46. W. Frącz and G. Janowski, *Mechanika*, **90**, 441 (2018).
47. A. B. Pillai, A. J. Kumar, and H. Kumarapillai, *3 Biotech*, doi: 10.1007/s13205-019-2017-9 (2020).
48. N. Israni, P. Venkatachalam, B. Gajaraj, K. N. Varalakshmi, and S. Shivakumar, *J. Environ. Manage.,* **255**, 109884 (2020).
49. M. L. Latour, M. Tarar, R. J. Hickey, C. M. Cuerrier, I. Catelas, A. E. Pelling, and G. Hall, *bioRxiv*, doi.org/10.1101/2020.01.15.906677 (2020).
50. S. Gorgieva, L. Girandon, and V. Kokol, *Mater. Sci. Eng. C*, **73**, 478 (2017).
51. G. Mutlu, S. Calamak, K. Ulubayram, and E. Guven, *J. Drug Deliv. Sci. Technol.,* **43**, 185 (2018).
52. N. F. Braga, D. A. Vital, L. M. Guerrini, A. P. Lemes, D. M. D. Formaggio, D. B. Tada, T. M. Arantes, and F. H. Cristovan, *Biopolymers*, doi: 10.1002/bip.23120 (2018).
53. J. Wangler and R. Kohlus, *Chem. Eng. Technol.,* **40**, 1552 (2017).
54. T. L. de A. Montanheiro, L. S. Montagna, V. Patrulea, O. Jordan, G. Borchard, R. G. Ribas, T. M. B. Campos, G. P. Thim, and A. P. Lemes, *Polym. Test.,* **79**, 106079 (2019).
55. K. Nisogi, O. Satoshi, S. Kobayashi, K. Kuroda, and T. Okamoto, *Mater. Sci. Forum*, **985**, 64 (2020).
56. M. Kouhi, M. Fathi, M. P. Prabhakaran, M. Shamanian, and S. Ramakrishna, *Appl. Surf. Sci.,* **457**, 616 (2018).
57. R. S. Ambekar and B. Kandasubramanian, *Ind. Eng. Chem. Res.,* **58**, 6163 (2019).
58. H. Tohidlou, S. S. Shafiei, S. Abbasi, M. Asadi-Eydivand, and M. Fathi-Roudsari, *Fiber. Polym.,* **20**, 1869 (2019).
59. A. P. M Madrid, S. M. Vrech, M. A. Sanchez, and A. P. Rodriguez, *Mater. Sci. Eng. C*, **100**, 631 (2019).
60. S. Saska, L. C. Pires, M. A. Cominotte, L. S. Mendes, M. F. de Oliveira, I. A. Maia, J. V. L. da Silva, S. J. L. Ribeiro, and J. A. Cirelli, *Mater. Sci. Eng. C*, **89**, 265 (2018).
61. S. Mondal and U. Pal, *J. Drug Deliv. Sci. Technol.,* **53**, 101131 (2019).
62. M. Pilia, T. Guda, and M. Appleford, *Biomed Res. Int.,* doi: 10.1155/2013/458253 (2013).
63. M. Hassan, K. Dave, R. Chandrawati, F. Dehghani, and V. G. Gomes, *Eur. Polym. J.,* **121**, 109340 (2019).